Equalisation of Archival Microscopic Images from Immunohistochemically Stained Tissue Sections

URSZULA NEUMAN[1,3,*], ANNA KORZYŃSKA[1], CARLOS LOPEZ[2], MARYLÈNE LEJEUNE[2], ŁUKASZ ROSZKOWIAK[1], RAMON BOSCH[2]

[1]*Nałęcz Institute of Biocybernetics and Biomedical Engineering,*
Polish Academy of Sciences, Warsaw, Poland
[2]*Molecular Biology and Research Section Hospital de Tortosa Verge de la Cinta,*
Tortosa, Spain
[3]*University of Nottingham, Jubilee Campus, Nottingham, United Kingdom*

A method of image equalisation that reduces non-uniformity of light distribution caused by optical devices and dust on camera sensors is presented. The method explores non-uniformity which occurs in archival images captured by a typical optical set which consists of a light microscope and a digital camera. A sufficient number of images with low density of foreground objects has been used to extract a global map of non-uniformity of the particular microscope and camera. The proposed method consists of two steps: – (1) extraction of the map of non-uniformity based upon a set of chosen images and – (2) correction of images acquired by the optical set. The global map is created based upon a modified value layer, the third layer of HSV colour space. The proposed method has been tested on images of immunohistochemically (IHC) stained samples of a biopsy tissue, and it has been validated using an image segmentation method developed earlier. The results of the light distribution equalization, as well as the equalized images segmentation turn out to be more similar to the reference method results (namely the manual counting results), than the results of the original images segmentation. The equalization method can be used for other types of images, but all of them should be acquired by the same optical set.

K e y w o r d s: immunohistochemically stained images, image light distribution, image equalization

1. Introduction

Immunohistochemically (IHC) stained tissue samples are used by pathologists to evaluate various types of cancer. For example, the aggressiveness and the

prognosis of follicular lymphoma and breast cancer tissue sections are evaluated using the IHC images [1, 2] stained with DAB (3,3'-diaminobenzidine) and contra-stained with haematoxylin (DAB&H) [3, 4]. The score of immunopositive cells' nuclei (brown objects) in the assumed area of interest and the architecture of the tissue sample are taken into account during the evaluation process. It can be done directly with a microscope or using a previously collected set of digital images of samples. Objects in digital images can be counted with [5–11] or without [12–14] a support of image processing methods which automate completely or incompletely this time consuming subjective work. The stained samples should be evaluated directly under a microscope, according to the WHO procedure [1, 2]. But with a development of image processing technologies, the direct observation of the samples can be supported by image analysis and processing methods using the digitalized version of the samples in both cases: in the case of cytological [15–19] and histological [4, 20–22] diagnosis and research. Defined so far image processing methods are not sufficiently effective yet, but further work on them should bring better results. The digital version of the samples allows pathologists not only (1) to come back to the chosen parts of a sample and (2) to make remote analyses by more than one lab worker (using tele-pathology facilities) but also (3) to create a good documentation of patient's illness history. Moreover, the archival images can be an interesting study subject, e.g. in the patient survival analysis. Computer-assisted cancer diagnosis, prognosis and treatment become the future of pathologist's and oncologist's work.

The method of improvement of the DAB&H stained digital images, which have been acquired with a particular optical set, is proposed in the paper. It is extremely important when computer-assisted counting methods are used, as colours allow to differentiate between immunereactive and not immunoreactive cells' nuclei.

The problem of digital image quality improvement is an extremely important part of image standardization process when dealing with virtual microscopy, what is discussed by Kayser et al. [23–25] and other authors [9, 20, 21, 26, 27]. Various correction methods are proposed in the literature. Some of them require a specific scene that usually has to be uniformly lit [28–32], others use a single image and create a function that is fit to this specific image using various methods of optimization [33, 34]. There are also methods that use sequences with overlapping scenes [35, 36].

Rolling Ball method [37], the most commonly used correction method, is available in ImageJ as a tool for background subtraction. It uses morphological operations to normalize the background of a single image and obviously works well under specific restrictions in the distribution and density of objects and in specific background variability.

The method proposed in the paper is a tool for creation a map of non-uniformity in light distribution across an image plane based upon a set of more than 100 digital microscopic images captured using a particular camera connected with a microscope. The system used to collect the images is not available currently in its original shape

(e.g. it is under construction). Hence, the correction methods that require a strictly defined scene and the methods that require overlapping scenes cannot be used. Those methods which use only one image to build the whole model of light distribution are suitable, if foreground objects of an image are loosely distributed and their size is small enough in comparison to changes of the image background intensity. Then it is possible to find a structural element size that erase the foreground objects without blurring the background intensity changes. However, there may be some great dust spots on optical elements of the capturing set which will not be reduced by this method.

In the proposed method the map of non-uniformity in the light distribution is calculated based upon a set of images with low or medium density of foreground objects, which can touch each other and may even constitute big nuclei clusters. As the construction set contains many images with random foreground objects location, the information that any particular point on the map belongs e.g. to the background, repeats itself in several images. In all images the method allows to detect small underexposed areas, which indicate the presence of contaminations in the optical path and in the camera sensors area.

The map of non-uniformity can be used to correct every image captured by the same optical set.

2. Biological Background

Quality of digital images depends on: both: (1) the process of image capturing, and: (2) the complicated and multistage process needed to obtain a immunohistochemically stained tissue sample.

The process of samples preparation starts from creation of a paraffin-embedded block from a tissue taken from a patient's body. Next, it is sectioned normally in a range from 2 to 6 μm and put on a glass. The slices are stained immunohistochemically with antibodies merging the protein which is specific for cells' nuclei in particular cancer. In this investigation the indirect staining is used, in which two types of antibodies are needed: (1) the first one is directly connected with the cellular protein (Ki67 or FOXP3), and (2) the second one, conjugated to a horseradish peroxidise (HRP) labelled polymer, is connected to the first one. The reaction of the enzyme with the substrate-chromogen DAB results in a brown colour precipitate at the antigen site (in this study DAB stains the immunopositive nuclei brown). Then the immunonegative nuclei are contra-stained blue with haematoxylin. Two images captured experimentally are presented in Fig. 1.

Some of the prepared samples are very pale (all colours are unsaturated, whitened as in Fig. 1A), while others are coloured intensively (with saturated blue, brown or both of them, as in Fig. 1B), what emphasizes the problem of how to set the camera settings to capture the homogeneous images from a set of nonhomogeneous samples. Intensity of the colours in a digital image depends on the process of staining,
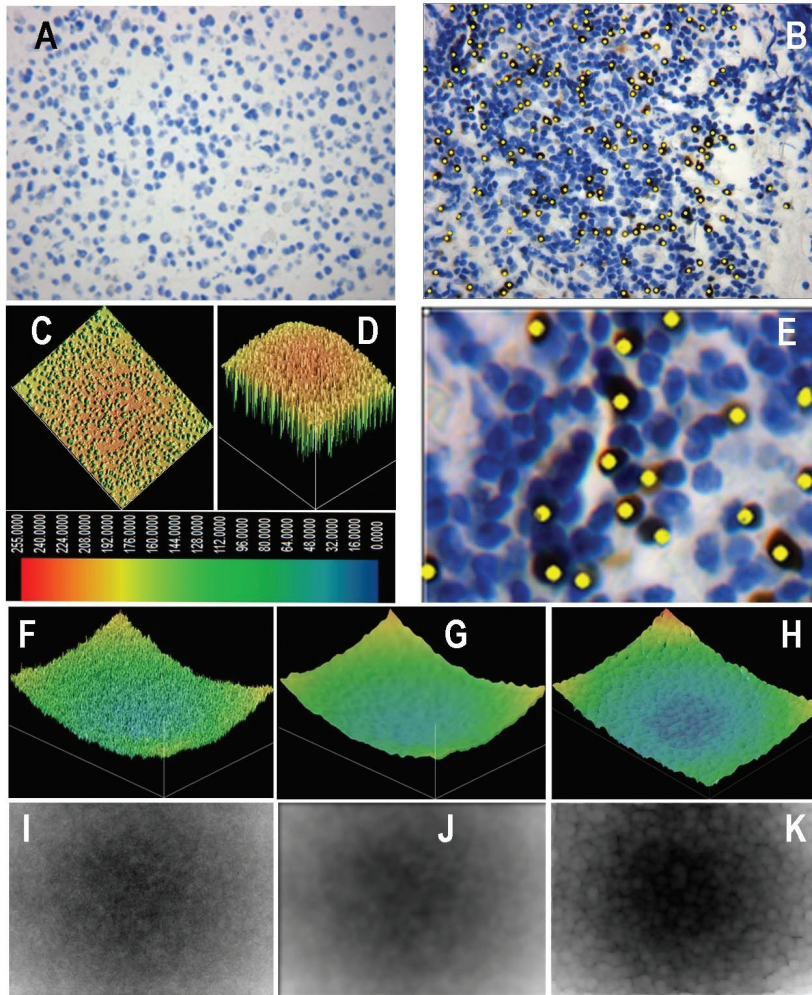
Fig. 1. Images and maps examples:
- image A – with blue coloured cells' nuclei only – immunonegative objects only;
- image B – with blue and brown coloured cells' nuclei – immunonegative and immunopositive for which yellow marks imposed by an operator using Image-Pro Plus software;
- image E – upper left corner of image B to show dim corners and a similarity of dark blue and dark brown nuclei in this region;
- C and D – image A shown as 3D function plot from two different elevation angles with pixel values shown according to the colour scale presented under images;
- F, G and H – shows 3D plot of maps of light distribution presented in images: I J and K;
- I, J and K – show 3 maps of light distribution constructed as the grey scale images F – by the proposed method without the final blurring, G – with the final blurring an H using the rolling ball method. All maps and 3D plots of light distribution in the optical device show an uneven illumination in corners and light spots in the middle. All of them are rescaled (in order to highlight the vignette pattern), so that the maximal value of each map gets the maximal displayable value and the minimal value gets value 0, while the range of grey scale levels is from 1 up to 70

described above, on the microscope (optical properties of the light pathway and the light itself) and the camera quality and on their actual settings (mainly on the chosen time of exposure). Setting of the camera ISO, white balance, and deep of field can unify some colours or shadows (e.g. colour of the immunoreactive object) over others (for example background or contra-stained objects).

Variation in the colours of the immunoreactive nuclei in the analysed archival set of images is large, from intensive orange, through intensive brown to dark brown (see Fig. 1E). That is typical when the number of chemical substrates is not stechiometric. A close similarity between the dark brown colour of immunopositive nuclei and the dark blue colour of immunonegative nuclei can be observed. Vignette (dim corners), introduced into the digital images by the optical set, makes differentiation between both types of nuclei very difficult, as it is hard to distinguish dark blue objects from dark brown ones crowded in the corners.

Proposed method which would reduce the nonhomogeneity in the light distribution, which is visible as vignette and artefacts (spots on the optical devices) should be verified counting the immunoreactive nuclei both (1) manually with a support of computer and (2) automatically using image processing methods with and without non-uniformily reduction.

3. Images

The digital images of the IHC samples have been provided by Hospital de Tortosa Verge de la Cinta, Spain, as a collection of patients' data from years 2005-2010. The microscope used to capture the images – Leica DMLB2 (LeicaMicrosystemsWetzlar GmbH, Wetzlar, Germany) was connected with the digital camera DFC320 (Leica Microsystems Digital Imaging, Cambridge, UK). Each of the collected images (1550 x 2088 pixels) shows a rectangular part of a sample (size 3.8 mm x 2.8 mm). The images have been stored as tiff, 24 bits pixels (8 bit/channel).

Patient samples already diagnosed by pathologist directly counting the brown-stained nuclei located in an assumed area of each sample and evaluating the tissue architecture was used for image processing analysis. Then for each sample a series of the digital images of several locations has been captured for the research purpose.

4. The Proposed Method

The proposed algorithm consists of two modules: the map creation module and the image correction module.

The map creation module uses those images from the big given image set which have a low or medium density of foreground objects, that is both immunopositive

and immunonegative cells' nuclei dispersed or clustered. In this case, 100 images with density of the objects similar to that observed in Fig. 1A and B have been used to create the map which shows characteristics of a light distribution presented in Fig. 1 from F to K. The presented method uses saturation layers of images to separate information about the clear background location and value layers to detect information about the lighting position in images.

The module of image correction improves a single image using the map produced in the first module. It can correct any image captured with the particular optical set.

Both modules are discussed below in detail.

4.1. The Map Creation Module

The map creation module consists of the following steps:

I.   For each image from the images classified to the set of n images used to construct the map:

  1. The colour space of each image i is converted from RGB (red, green, blue) to HSV (hue, saturation Si , value Vi)
  2. Channels Vi and Si are selected (where i is the image number in the set and can take a value from 1 to n)
  3. Channel Vi is modified by removing saturated points based upon a test of Si layer (for the images that have saturation in the range from 0 to 1; pixels with saturation less than 0.1 are suppressed to black).

II.   Next:

  1. Matrix q and empty map M of the size of a single 8-bit greyscale image are created (range (x,y))
  2. For each position (x,y) a sum of values of V layers and the number of non-modified layers (how many layers in this position have value different than 0) are calculated and saved in matrix q
  3. The result of dividing the sum by corresponding $q(x,y)$ is saved in map M according to the equation:

$$M(x, y) = \frac{\sum_{i=1}^{n} Vi(x, y)}{q(x, y)} \tag{1}$$

  4.   Final map M, which resembles an 8-bit deep greyscale image, is additionally slightly blurred by the LowPassGaussian filter to make it smoother.

The final map constructed for the archival images (see section 3) is presented in Fig. 1J. The presented map is rescaled in order to highlight the vignette pattern. The maximal value of the map gets the maximal displayable value and the minimal value of the map gets value 0, while in the microscopic images the range between the mean of V-channel value in the corners and in the centre is about 70 levels. The

map presented in Fig. 1F is textured, because it is before the smoothing step of the procedure (see II 4).

4.2. The Image Correction Module

The correction module uses the map *M* shifted and inverted to correct image *I* captured with the optical device, characterized by the map *M.* It is performed in the following steps:

1. Values of map *M* are shifted to make the minimal value of *M* equal 0:

$$Mshift\ (x,y) = M(x,y) - min(M) \tag{2}$$

2. The colour space of image *I* is converted from RGB to HSV
3. The value layer *(VI)* of image *I* is modified by adding a negation of *Mshift*

$$VII = VI + negative(Mshift) \tag{3}$$

4. The value layer (*VII)* is modified by adjustment to the whole range of the grey scale (allowing not more than *1%* of pixel would become saturated)
5. *H* and *S* channels are combined with the modified value layer (*VII)* and the image is converted back to RGB.

5. Evaluation of the Proposed Image Correction Method

Evaluation of the proposed correction method is done on various levels: (1) by visual assessment of maps constructed by different methods, (2) by comparison of the results of manual counting to automated counting done with the method proposed earlier, and (3) by examining the effectiveness of the correction method in the images of various characteristics. This last examination is described in the next section while the previous below.

The map of the light distribution calculated using the proposed method, based upon 100 selected images (the creation set) is compared to several maps created using an algorithm, called Rolling Ball, and implemented in ImageJ [37]. The Rolling Ball algorithm, which is designed to create a single image using only this image, has been used to improve several images chosen from the creation set. The images have been chosen according to the method assumptions – the images with a small amount evenly distributed foreground objects are expected. The Rolling Ball algorithm subtracts a background from an image. The background is created based only upon the information from the image. Hence, correction works well only if fluctuations of the background intensity are low and the largest foreground objects or clusters of foreground objects are much smaller than the fluctuations. It is because the size of

the maximal foreground object decides about the size of a structural element used by the Rolling Ball method for morphological closing and opening operations [38–43]. The operations remove the objects from the image and interpolates values of the background under the disappearing objects based upon the nearest neighbourhood background. An image and it's background map constructed based upon it using the Rolling Ball method calculated for V-layer of this image are presented in Fig. 1A and K respectively while Fig.1 H presents the map as the image function.

The results of the Rolling Ball algorithm, presented in Fig. 1K and H are juxtaposed with the final map constructed by the proposed method Fig. 1 J and G. Visual comparison of both maps shows a similarity of their general pattern with the dim corners and the intensively brightened centre, while their smoothness is different. The final map obtained using the proposed method is smoother in comparison to the Rolling Ball map, where size and shape of the used structural element introduce the specific pattern. All images in Fig. 1 are rescaled using the analogous linear histogram enlarging as it is described above.

Exact visual inspection of the Rolling Ball map shows that it contains a pattern resulting from a chosen shape and size of the structural element used in the morphological operations. It means that a different shape and/or size of the structural element would produce different results. As the shape and/or size of this element are strictly dependent on the shape and/or size of the largest foreground objects the method would only be efficient for a subset of the archival images. Many images we deal with are complicated, with medium or even high density of objects mostly clustered.

It is clearly visible that both the Rolling Ball method results and the proposed method results detected a similar vignette pattern introduced by the optical set. Both methods detect a similar difference (in location and values) between the intensity of the centre and the corners of the images. But the proposed method, thanks to the averaging process of about 100 images, results with the more uniform and smooth map and it can deal with more complicated images, e.g. images having medium density of objects or even clusters of objects. Finally the result of the proposed method can be used to improve even very complicated images, which have been excluded from the map creation module. So, the method uses images with low or medium density of objects, even with clusters, to create the map and then uses it to correct all images, both included and excluded from the set used to create the map of the light distribution.

The results of the proposed correction method are then evaluated using an automated segmentation method earlier prepared and described in [44]. The immunoreactive nuclei in the corrected and uncorrected images are counted using the automated segmentation method, which is based upon colour adaptive threshold operations [44–47]. First, the objects are thresholded. Then, the objects bigger than the assumed size are divided according to their shapes using the watershed method and several basic morphological operations [48–54].

Average results of triple manual nuclei counting, done by two experts (mini-mization the intra- and inter- observer variability), are used as the reference for automated counting. Image-Pro Plus (Media Cybernetics INC) software has been used by the experts to count brown objects in the uncorrected images. This software offers a manual supporting tool to mark objects which should be counted. Fig. 1 B and C present brown nuclei marked manually.

The number of the selected brown objects, using the automated method for both uncorrected and corrected images, is compared to the manually obtained results. If the counting result obtained for a corrected image is closer to the manual counting result than the result obtained for the uncorrected one, the correction method is suitable and positively influences the image appearance in the context of the colour segmentation of brown objects. Otherwise, if the manual results are close to the results obtained for the uncorrected image, the proposed correction method is not effective.

In general, no influence and positive influence of the image correction perform-ance are observed in 66% of the tested images, mostly because the number of false negative cases after the image correction decreases, while the negative influence of image correction is observed in 34% of the images.

6. Deep Analysis of Effectiveness of the Proposed Method

Evaluation of the proposed method of the IHC stained image correction described above shows that the method is efficient in some but not in all cases. It is interest-ing for which images the correction improves results of automated counting of the immunoreactive nuclei. As the automated segmentation method extracts an object according to its colour, it seems that the colour saturation is the crucial factor which influences the results.

The set of 50 images has been divided into three subsets: (1) the subset of the very pale images (whitened), (2) the subset of the images with saturated colours, and (3) the subset of the dark low saturated images (blackened), according to the mean values of saturation layer (channel) of the HSV colour model. The mean value and the standard deviation of the image saturation have been calculated for each image from the test set and its value has been 180 ± 13. If an image mean saturation is in the range given by the general mean plus minus the standard deviation, it is categorized as the saturated image. Otherwise it goes to the set of the dark (low saturated and low share of white) or pale (low saturated and whitish) images. 8 (16%) from 50 images has been categorized as pale, 33 (66%) as saturated and 9 (18%) as dark.

Figure 2 has been introduced to show trends of the results in each group. There are three bars presented in this figure, which correspond to three subsets: the left one corresponds to the subset of the dark images, the middle one to the pale images and the right one to the saturated images. Each bar consists of three parts which differ

in colour. The light grey part corresponds to the percentage of the improved images, for which the amount of brown objects calculated after the image correction is closer to the manual counting results, than for the uncorrected images. The dark grey part corresponds to the percentage of images for which an influence of the correcting method is not essential, while the middle grey part corresponds to the percentage of images for which the correction appears to be useless.
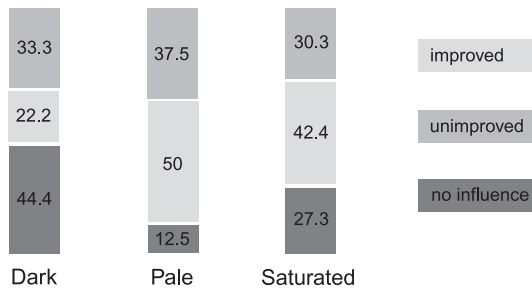
Fig. 2. The results for each subset of the images: the left bar for the subset of the dark images, the middle bar for the pale images and the right bar for the saturated images; the shades of grey colour subsections correspond to the percentage of various effectiveness of the method: light grey colour corresponds to the percentage of the images highly improved, the dark grey colour subsection corresponds to the percentage of the images for which the correction has not influenced the result of object counting and, finally, the middle grey colour subsection corresponds to the images for which results have been unimproved

In general, for 30–38% of the images the correction appears to be useless, while for the rest the use of correction is justified.

7. Conclusions

The digital images of tissue samples stained by IHC used to diagnose a cancer tissue section, to determine the prognosis and the appropriate treatment should be as good as possible, regardless of whether they are evaluated both by a human and by an automatic method. So, a big effort should be put to prepare the samples and capture the images. During the process of capturing the most important for the image quality is to adjust the deep of field and to select an appropriate exposure. A badly selected exposure results in pale or dark images (whitened or blackened), what causes additional problems with automated counting the immunopositive objects. The collection of the archival digital images, which constitutes documentation of the interesting cases, could be improved using the method proposed in this paper.

Direct observation with microscope allows to penetrate the deep of field in a sample better than with a digital camera, particularly if a pathologist uses the

micrometric knob interactively. But the digital image captured by a camera, examined on a computer screen, despite showing a stable narrow deep of field gives other advantages. Pathologists may be supported or even lead by software, which performs the image processing, selection of information, highlighting relations between the objects, measuring and counting the detected objects automatically.

The proposed method of image correction improves quality of the digital images by removing vignette – dim corners – caused by some nonuniformity in the light distribution in the microscope and camera optics. Due to vignette, dark blue nuclei in the corners become nearly black and can be confused with brown nuclei. Also dust on the sensors can introduce spots wrongly classified as nuclei. The proposed method of the image improvement works as adjusted to the enhancement of mean local contrast. The image improvement is more visible in the saturated (well exposed) and pale (overexposed) images than in the dark (underexposed) images. The dark images have been captured with a big lost of information about colour of foreground objects and the correction method cannot supply costed details.

In the proposed method it is assumed that the map of light distribution is constructed based upon a set of images with low or medium density of randomly distributed foreground objects, localized in clusters or not and captured by a particular optical set. This assumption is milder than applied in many methods described in the literature (e.g. the Rolling Ball method). Additionally, for a particular microscope and a camera, the map of nonuniformity in the light distribution can be used to correct various images (not necessarily IHC stained images) captured by this set. Moreover, the proposed method of construction of the map correction, based upon a big collection of archival images, can be used for other optical sets and other types of digital images.

References

1. Fattaneh A.T., Devilee P. (Eds.): Pathology & Genetics of Tumours of the Breast and Female Genital Organs, 2003, IARCPress, Lyon.
2. Swerdlow S.H., Campo E., Harris N.L. et al. (Eds.): WHO Classification of Tumours of Haematopoietic and Lymphoid Tissues, IARC Press, Lyon, 2008.
3. Schulerud H., et al.: A review of caveats in statistical nuclear image analysis. Analit. Cell Pathol. 1998, 16, 63–82.
4. Alvaro T., Lejeune M., Salvado M.: Immunohistochemical patterns of reactive microenvironment associated with the clinic-biological behavior in follicular lymphoma patients. J. Clin. Oncol. 2006, 24(34), 5350–5357.
5. Comaniciu D., Meer P.: Cell image segmentation for diagnostic pathology. In Suri J.S., Setarehdan S.K. (Eds.), Advanced algorithmic approaches to medical image segmentation: state-of-the-art application in cardiology, neurology, mammography and pathology, 2001, 541–558.
6. Markiewicz T., Wisniewski P., Osowski S., Patera J., Kozlowski W., Koktysz R.: Comparative analysis of methods for accurate recognition of cells through nuclei staining of KI-67 in neuroblastoma and estrogen/progesterone status staining in breast cancer. Analyt. Quant. Cytl. Histol. 2009, 31(1), 49–62.

7. Markiewicz T., Osowski S., Pater J., Kozlowski W.: Image processing for accurate cell recognition and count on histologic slides. Anal. Quant. Cytol. Histol. 2006, 28(5), 281–291.

8. Lopez C., Lejeune M., Salvedo M.T., Escriva P., Bosh R., Pons L.E., Alvaro T., Roig J., Cugat X., Baucells J., Jaen J.: Automated quantification of immunohistochemical markers with different complexity, Histochem. Cell Biol. 2008, 129(3), 379–287.

9. Rojo M., Bueno G., Slodkowska J.: Review of imaging solutions for integrated quantitative immunohistochemistry in the pathology daily practice. Folia Histochemica et Cytobiologica 2009, 47(3) 349–354.

10. Seidal T., Balaton A., Battifora H.: Interpretation and quantification of immunostains. Am. J. Surg. Pathol. 2001, 25, 1204–1207.

11. Yaziji H. et al.: Diagnostic immunohistochemistry: What can go wrong? Adv. in Anat. Pathol. 2006, 13(5), 238–246.

12. Kruś S., Skrzypek-Fakhoury E.: Clinical Pathology, Wydawnictwo Lekarskie PZWL, Warszawa, 2007 (in Polish).

13. Gil J., Wu H.-S.: Applications of image analysis to anatomic pathology: Realities and promises. Cancer Investigation 2003, 21(6), 950–959.

14. Gil J., Wu H., Wang B. Y.: Image analysis and morphometry in the diagnosis of breast cancer. Microscopy Research and Technique 2002, 59(2), 109–118.

15. Korzynska A., Strojny W., Hoppe A., Wertheim D., Hoser P.: Segmentation of microscope images of living cells. Pat. An. & App. 2007, 10, 301–319.

16. Korzynska A., Hoppe A., Strojny W., Wertheim D.: Investigation of a combined texture and contour method for segmentation of light microscopy cell images. Proc. Second IASTED International Conference on Biomedical Engineering, 2004, 234–239.

17. Korzynska A., Iwanowski M.: Multistage morphological segmentation of bright-field and fluorescent microscopy images. Opto-Electronics Review 2012, 20, 174–186.

18. Koprowski R., Wrobel Z.: The cell structures segmentation. Springer-Verlag, 2005, Advances in Soft Computing, 569–576.

19. Dulewicz A., Pietka D., Juszczak P.: Digital image analysis in research and diagnosis of urinary bladder cancer. In Bladder Cancer: Etymology, Diagnosis and Treatment (ed.) Nilsson W.E. Nova Science Biomedical Books, New York, 2010.

20. Markiewicz T., Osowski S., Patera J., Kozlowski W.: Image processing for accurate cell recognition and count on histologic slides. Analyt. Quant. Cytl. Histol. 2006, 28(5), 281–291.

21. Roux L., Tutac A., Lomenie N., Balensi D., Racoceanu D. et al.: A cognitive virtual microscopic framework for knowledge-based exploration of large microscopic images in breast cancer histopathology. Engineering in Medicine and Biology Society, 2009. EMBC 2009. Ann. Intern. Conf. IEEE, 2009, 3697–3702.

22. Grala B., Markiewicz T., Kozlowski W., Osowski S., Slodkowska J., Papierz W.: New automated image analysis method for the assessment of ki-67 labeling index in meningiomas. Folia Histochemica et Cytobiologica 2009, 47(4), 587–592.

23. Kayser K. et al.: Image standards in Tissue-Based Diagnosis (Diagnostic Surgical Pathology), Diagnostic Pathology, 2008.

24. Kayser K., Radziszowski D., Bzdyl P., Sommer R., Kayser G.: Towards an automated virtual slide screening: theoretical considerations and practical experiences of automated tissue-based virtual diagnosis to be implemented in the internet. Diagnostic Pathology 2006, 1, 1–10.

25. Kayser K., Radziszowski G., Bzdyl D., Sommer P., Kayser G.: Theory and implementation of an electronic, automated measurement system for images obtained from immunohistochemically stained slides. Anal. Quant. Cytol. Histol. 2006, 28(1), 27–38.

26. Klapper W. et al.: Ki-67 as a prognostic marker in mantle cell lymphoma-consensus guidelines of the pathology panel of the European mcl network. J of Hematopathology 2009, 2, 103–111.

27. Bartels P.H., Montironi R., D. da Silva V., Hamilton P.W.: Thompson D., Vaught L.: Tissue architecture analysis in prostate cancer and its precursor: An innovative approach to computerized histometry. Rur. Urol. 1999, 35, 484–491.

28. Asada N., Amano A., Baba M.: Photometric calibration of zoom lens systems. Proc. Int. Conf. on Pattern Recognition 1996, 186–190.

29. Kang S., Weiss R.: Can we calibrate a camera using an image of a flat textureless lambertian surface? European Conf. on Computer Vision, II, 2000, 640–653.

30. Sawchuk A.A.: Real-time correction of intensity nonlinearities in imaging systems. IEEE Trans. on Computers, 1977, 26(1), 34–39.

31. Yu W.: Practical anti-vignetting methods for digital cameras. IEEE Trans. on Cons. Elect., 2004, 50, 975–983.

32. Korzyńska A., Neuman U., Lopez C., Lejeune M., Bosch R.: The Method of Immunohistochemical Images Standardization. In: R.S. Choras (ed.): Image processing & Communications Challenges 2, AISC 84, Springer-Verlag, Berlin, Heidelberg, 2010, 213–221.

33. Zheng Y., Lin S., Kang S.B.: Single-image vignetting correction. In CVPR, 2006, 1, 461–468.

34. Zheng Y., Yu J., Kang S.B. et al.: Single-image vignetting correction using radial gradient symmetry. In CVPR, IEEE, 2008, 1–8.

35. Goldman D., Chen J.: Vignette and exposure calibration and compensation. In ICCV, 2005, 899–906.

36. Choi H.J., Choi I.H., Cho N.H., Choi H.K.: Colour image analysis for quantifying renal tumor angiogenesis. Analyt. Quant. Cytl. Histol. 2005, 27, 43–51.

37. Litvinov A., Schechner Y.: Addressing radiometric nonidealities: A unified framework. In CVPR, 2005, 52–59.

38. Sternberg S.R.: Biomedical Image Processing. Computer, 1983, 22–34.

39. Iwanowski M.: Morphological methods in digital image processing, AOWEXIT, Warszawa, 2009 (in Polish).

40. Nieniewski M.: Mathematical morphological methods in image processing, PLJ, Warszawa, 1998 (in Polish).

41. Soille P., Iwanowski M.: Morphological Refinement of an Image Segmentation. Lecture Notes in Computer Science, Springer-Verlag Berlin Heidelberg, 2005, 538–545.

42. Iwanowski M., Serra J.: The morphological-affine object deformation, Mathematical Morphology and its Applications to Signal and Image Processing. Kluwer Academic Publishers, 2000, 81–90.

43. Markiewicz T.: Using matlab software with tomcat server and java platform for remote image analysis in pathology. Diagnostic Pathology 2011, 6(1), 18.

44. Neuman U., Korzyńska A., Lopez C., Lejeune M.: Segmentation of Stained Lymphoma Tissue Section Image. In: E. Pietka, J. Kawa (eds.): Information Technologies in Biomedicine AISC 69, Springer-Verlag, Berlin, Heidelberg, 2010, 101–113.

45. Du X., Dua S.: Segmentation of fluorescence microscopy cell images using unsupervised mining, Open Med. Inform. J. 2010, 4, 41–49.

46. Czajkowska J., Badura P., Pietka E.: 4d segmentation of ewing's sarcoma in MR images. in Information Technologies in Biomedicine, ser. Advances in Intelligent and Soft Computing, E. Pietka, J. Kawa, Eds. Springer Berlin / Heidelberg, 2010, 69, 91–100.

47. Pham D. et al.: A survey of current methods in medical image segmentation. Ann. Rev. Biomed. Eng. 2000, 2, 315–338.

48. Fu K., Mui J.: A survey on image segmentation, Pattern Recogn. 1981, 13, 1, 3–16.

49. Serra J., Vincent L.: An overview of morphological filtering. Circuit Systems Signal Processing, 1992, 11(1).

50. Serra J.: Image analysis and mathematical morphology. Academic Press 1, 1983.

51. Serra J.: Image analysis and mathematical morphology. Academic Press 2, 1988.

52. Vincent L.: Morphological Greyscale Reconstruction in Image Analysis: Applications and Efficient Algorithms. IEEE Trans. Image Processing 1993, 2(2).

53. Soille P.: Morphological Image Analysis: Principles and Applications. Springer-Verlag. 2004.

54. Wróbel Z., Koprowski R.: Image processing in the MATLAB software, Wydawnictwo Uniwersytetu Śląskiego, Katowice, 2001 (in Polish).